Acta Crystallographica Section D
Biological Crystallography
ISSN 0907-4449

New kinase regulation mechanism found in HipBA: a bacterial persistence switch

Artem Evdokimov,*‡ Igor Voznesensky,‡ Kimberly Fennell, Marie Anderson, James F. Smith and Douglas A. Fisher

Pfizer Inc., 558 East Point Road, Groton, Connecticut, USA

‡ These authors contributed equally.

Correspondence e-mail: artem@xtals.org

Received 30 March 2009
Accepted 18 May 2009

PDB Reference: HipBA, mercury derivative, 2wiu, r2wiusf.

Bacterial persistence is the ability of individual cells to randomly enter a period of dormancy during which the cells are protected against antibiotics. In *Escherichia coli*, persistence is regulated by the activity of a protein kinase HipA and its DNA-binding partner HipB, which is a strong inhibitor of both HipA activity and *hip* operon transcription. The crystal structure of the HipBA complex was solved by application of the SAD technique to a mercury derivative. In this article, the fortuitous and interesting effect of mercury soaks on the native HipBA crystals is discussed as well as the intriguing tryptophan-binding pocket found on the HipA surface. A HipA-regulation model is also proposed that is consistent with the available structural and biochemical data.

1. Introduction

After exposure to a clinically effective concentration of antibiotic, virtually all cells in a clonal population of bacteria are killed. However, a small fraction of cells (10^{-5}–10^{-6} times the original amount) survive for extended periods of time in a quiescent state, a phenomenon that is known as bacterial persistence (Jayaraman, 2008). Persistence is distinct from antibiotic resistance: when 'persisters' are re-cultured in the absence of antibiotic, their progeny are as sensitive to the antibiotic as the cells in the original population. Persistence is not selective with respect to the chemical class of the antibiotic agent: it seems to be one of the generic strategies that bacteria have evolved to survive periodic environmental stress (Kussell *et al.*, 2005). The persistence phenomenon is clinically relevant in the recurrence of bacterial infections after ending antibiotic therapy and has been cited as one factor in the exceptional resistance of biofilms to antibiotic treatment (Brooun *et al.*, 2000; Lewis, 2008).

Moyed and coworkers (Black *et al.*, 1991, 1994; Moyed & Bertrand, 1983; Moyed & Broderick, 1986) were the first to describe some of the protein components that modulate the persister state in *Escherichia coli*. They discovered the *hip* operon, which encodes two proteins, HipA and HipB, that conceptually resemble a toxin–antitoxin pair. The toxin HipA has serine/threonine kinase activity, whereas the antitoxin HipB is a small helix–turn–helix (HTH) protein with dual functionality: it tightly binds to and inhibits HipA protein and it represses the *hip* promoter by binding to the upstream inverted DNA repeats. While this manuscript was in preparation, the first link between HipA toxicity and its ability to promote persistence has been reported (Schumacher *et al.*, 2009). Apparently, HipA is capable of phosphorylating the elongation factor EF-Tu, which results in the latter being unable to bind aminoacyl-tRNA and to participate in translation. Schumacher and coworkers have solved the structure of the $HipBA_{D309Q}$–DNA complex as well as the structures of the $HipA_{D309Q}$–ATP and $HipA_{D309Q}$–AMPPNP–EF-Tu peptide complexes (Schumacher *et al.*, 2009). Unaware of this work, we have independently solved the X-ray crystal structure of the native HipBA complex and of its mercury derivative. Based on all the available data, we propose a HipA activity-regulation mechanism that has not previously been observed in other kinases.

© 2009 International Union of Crystallography
Printed in Singapore – all rights reserved

2. Experimental

2.1. Molecular cloning, protein production and crystallization

A detailed description of recombinant HipBA complex production has been deposited as supplementary material[1]. In brief, we amplified the entire *hip* operon from *E. coli* DNA by PCR and introduced a 6×His tag at the C-terminus of HipA. The operon was inserted into pET28a vector (Novagen) and the resulting construct was transformed into BL21 (DE3) *E. coli* (Invitrogen). By growing the cells in an autoinduction medium (EMD), we obtained 20–50 mg soluble HipBA complex per litre of culture, which we purified from the bacterial lysate by means of metal-affinity chromatography. We confirmed that the complex had 1:1 stoichiometry by means of SDS–PAGE and LC–MS analysis. Using the same methods, we were able to produce native HipA as well as the $HipA_{S150A}$ mutant. In the case of native HipA expression, the cell mass and protein yields were low owing to the expected toxicity of this protein.

We used a weighted average of theoretical A_{280} values for HipA and HipB to quantify the complex. Purified HipBA was concentrated to 10 mg ml^{-1} and subjected to an array of crystallization screens as follows: drops containing 0.6 µl protein solution and 0.6 µl reservoir solution were set up against a number of commercially available crystallization screens (Hampton Research, deCODE, Qiagen) in a 96-well hanging-drop format using a Mosquito (TTP LabTech) robot. A number of high-salt conditions produced crystals of varying visual appeal. We optimized several sodium tartrate or ammonium sulfate based hits until crystals of useful size were obtained. Since HipA is a kinase, we tested the effect of ATP and its analogues on crystallization and found it to be beneficial, with the best quality crystals being obtained in the presence of β,γ-methylene-substituted ATP (AMP-PCP). The final crystallization conditions were 2.0 *M* ammonium sulfate, 100 m*M* HEPES pH 7.5, 6% ethylene glycol mixed with 10 mg ml^{-1} HipBA supplemented with 3 m*M* AMP-PCP. The presence of both HipB and HipA in these crystals was confirmed by SDS–PAGE. Crystals of HipBA could be cryoprotected by brief immersion into mother liquor supplemented with 22.5% ethylene glycol; this was followed by flash-freezing in a nitrogen stream at 100 K.

2.2. X-ray studies of HipBA crystals and their heavy-atom derivatives

Numerous derivatives were tested, including compounds of mercury, platinum, osmium, lanthanides, lead, palladium and iodine. Successful incorporation of heavy atoms into HipBA crystals was accomplished both by slow soaking at a low reagent concentration (1 m*M*) and by rapid soaking (10–20 min; Sun & Radaev, 2002; Sun *et al.*, 2002) at reagent concentrations in the range 5–20 m*M* in mother liquor. Several derivative data sets were collected using our laboratory X-ray source. For synchrotron data collection, we soaked HipBA crystals in 10 m*M* ethylmercury phosphate or methylmercury acetate for 10 min.

Laboratory-based diffraction experiments were conducted using an FR-E X-ray generator and a Saturn CCD X-ray detector (Rigaku). The diffraction data used in this article were collected on National Synchrotron Light Source beamline X25 equipped with an ADSC Q315-R CCD detector. Data were collected as 0.5° oscillations totalling 360° with an exposure time of 1 s per oscillation. The crystal-to-detector distance was 170 mm. Owing to noticeable radiation-induced decay, only the first 145° of data were used. Indexing of diffraction images, integration and scaling of data were performed in *HKL*-2000 (Otwinowski & Minor, 1997).

Table 1
Essential crystallographic statistics.

Values in parentheses are for the highest resolution shell.

Wavelength (Å)	1.01
Resolution (Å)	2.40 (2.45–2.40)
Space group	$P4_222$
Unit-cell parameters (Å)	$a = b = 166.93$, $c = 124.575$
R_{merge} (%)	0.06 (0.29)
Unique reflections	68447 (6794)
Completeness (%)	99.3 (99.9)
$\langle I/\sigma(I)\rangle$	24.1 (3.8)
Multiplicity	6.0 (6.0)
R_{cryst} (%)	0.22 (0.25)
R_{free} (%)	0.26 (0.30)
Protein atoms	7549
Solvent atoms	283
Bond length r.m.s.d. (Å)	0.011
Bond angle r.m.s.d. (°)	1.26
Ramachandran preferred (%)	94.4
Ramachandran allowed (%)	5.6

2.3. Structure solution and refinement

Initially, we obtained phases for the HipBA crystal structure by means of MIR (neodymium, lead and platinum derivatives) using 3.5–4.0 Å resolution data collected on our laboratory X-ray source. The programs *SHELXD* (Sheldrick, 2008) and *SOLVE* (Terwilliger, 2004) were used to find heavy-atom sites; the program *SHARP* (Vonrhein *et al.*, 2007) was used to refine the phasing solution. The resulting maps were improved using the programs *SOLOMON* (Abrahams & Leslie, 1996) and *RESOLVE* (Terwilliger, 2004). While it was possible to perceive clear solvent–protein boundaries and some of the secondary structure in the MIR maps, we did not succeed in fully tracing the polypeptide chains. We used the mercury-derivative SAD synchrotron data to locate six partially occupied Hg sites (*SHELXD*) and generate phases using *SHARP*. Density modification by *SOLOMON* resulted in readily interpretable maps at 2.4 Å resolution. Automated polypeptide tracing (*ARP/wARP*; Perrakis *et al.*, 1999) successfully identified ∼65% of the residues; the remainder were built manually using the program *Coot* (Emsley & Cowtan, 2004). The resulting structure was refined against the mercury-derivative data. Several rounds of refinement (*REFMAC*; Murshudov *et al.*, 1997) and rebuilding were followed by a round of water-picking (*Coot*) and extensive geometrical analysis using *MolProbity* (Davis *et al.*, 2007) and *SFCHECK* (Vaguine *et al.*, 1999). The structure of unmodified HipBA was solved by direct substitution with one half of the Hg-HipBA structure with position adjusted to compensate for the space-group difference between the two crystals. Poor data quality necessitates considerable further refinement of this structure, which will be released at a later time. The mercury-derivatized HipBA structure was deposited with the RCSB (PDB code 2wiu).

3. Results and discussion

3.1. The curious effect of mercury salts on HipBA crystals

Large crystals of the HipBA complex were easily and reproducibly obtained in numerous salt-based conditions; however, their properties were far from optimal. Native HipBA crystals diffracted X-rays in a highly anisotropic fashion (Fig. 1*a*), which was not entirely surprising given their relatively high solvent content (71%). In the best direction diffraction spots could be observed at ∼2.6 Å resolution; however, in the worst direction there were hardly any useful

[1] Supplementary material has been deposited in the IUCr electronic archive (Reference: HV5130). Services for accessing this material are described at the back of the journal.

spots beyond 3.8 Å. This is not a consequence of crystal freezing since capillary-mounted crystals also produced anisotropic X-ray diffractograms. Our attempts to improve matters by means of controlled crystal desiccation, cryo-annealing or by changing the cryoprotectant did not result in success. While experimenting with various heavy-atom derivatives, we noticed a curious phenomenon: short-term exposure of HipBA crystals to methylmercury chloride or ethylmercury phosphate causes considerable improvement of their X-ray diffraction quality (Fig. 1*b*). At the same time, the asymmetric unit volume doubles and the crystal space group changes from the native $P422$ to $P4_222$. Prolonged treatment with mercury salts causes the diffractogram quality to deteriorate. We collected X-ray diffraction data from the mercury-derivatized crystals and readily solved the structure of the complex by the SAD technique. This structure has in turn enabled us to solve the native HipBA complex and to determine the nature of the space-group transition.

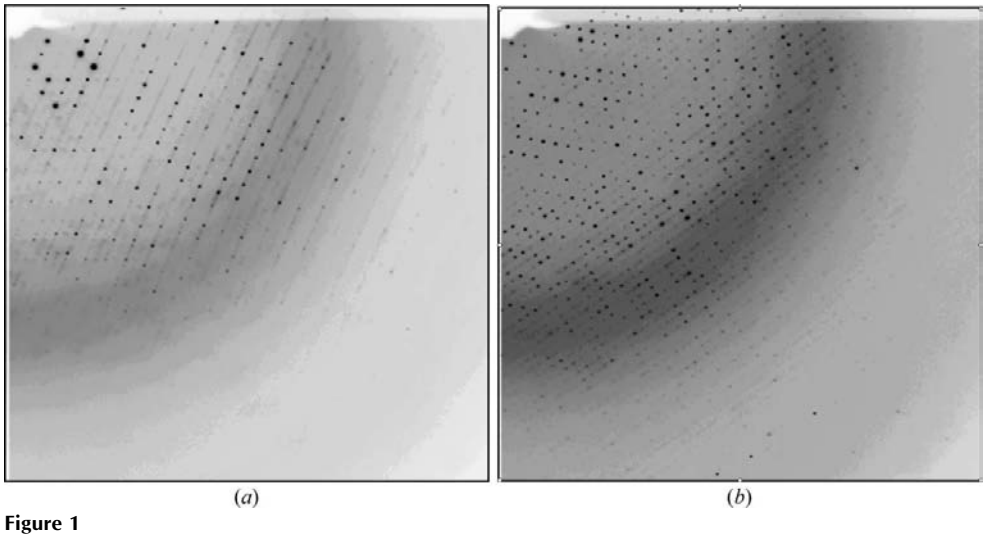

Figure 1
X-ray diffraction patterns collected from (*a*) native and (*b*) mercury-soaked HipBA crystals. The right edge of the images corresponds to ∼2.3 Å resolution.

In the native HipBA crystals the asymmetric unit is occupied by one half of the AB|BA heterotetramer, with the other half supplied by the crystal twofold symmetry. Mercury-salt treatment de-symmetrizes the two halves of the tetramer as follows: firstly, the attachment of mercury ions is somewhat uneven with respect to HipA monomers, and secondly, the HipA flexible region (residues 131–155) adopts two very different conformations in the two halves of the assembly (Fig. 2). We think that these two phenomena are linked: it is likely that mercury derivatization causes the flexible region to sample specific conformations more frequently. It is not clear how the attack of mercury ions on the fully symmetrical native heterotetramer in a symmetry-equivalent crystal environment results in an asymmetric attachment and in the subsequent conformational change of only one HipA molecule. We speculate that the process of de-symmetrization begins with the random derivatization of a few molecules at Cys168, which is located close to its own symmetry mate. This breaks the local symmetry and in turn results in preferential exposure and higher reactivity of additional sites, which causes further local loss of symmetry. Local rearrangement propagates through the remainer of the crystal like a domino effect, driving further derivatization in a specific direction. This phenomenon is transient; prolonged exposure to mercury salts results in full and uniform derivatization with concomitant loss of crystal diffraction quality.

3.2. Comparison with recently published structures

The structure of a $HipBA_{D309Q}$–DNA complex was reported by Schumacher and coworkers while our paper was in preparation. For the sake of brevity, we direct the reader

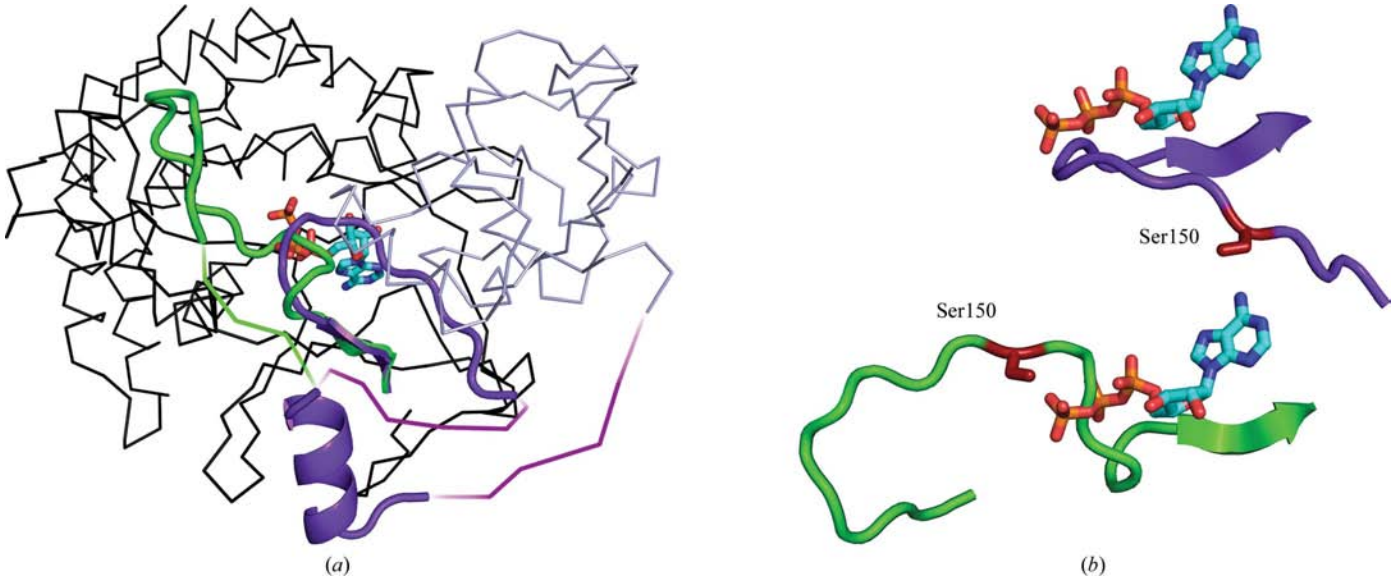

Figure 2
Two conformations of the flexible region (131–155) of HipA. (*a*) Two conformations superposed; (*b*) details of the Ser150 region for each conformation. The N-terminal and the C-terminal domains of HipA are shown as blue and black C^{α} traces, respectively. The two forms of the flexible region are shown in green and violet. The bound ATP molecule is shown as a CPK-colored ball-and-stick model and the side chain of Ser150 is shown in stick representation.

to the original paper (Schumacher *et al.*, 2009) for a detailed description of the complex, as our native HipBA structure can be superposed onto the previously reported structure with a C^{α} r.m.s.d. of 0.6 Å. It is remarkable that even though the HipB dimer bends its cognate DNA by ∼70°, the structure of HipB remains virtually unperturbed in the complex (C^{α} r.m.s.d. of 0.3 Å). The only areas of significant difference between the available HipA structures are the flexible 131–155 region, three loops (184–196, 263–271 and 357–362) that are disordered in one of the structures while visible in the other and the inter-domain connector 108–118, which is mostly disordered in our structures. Despite the presence of ATP analogues in our crystallization experiments, we did not observe these ligands in the active site of the enzyme, even though the active-site geometry does not differ significantly between the structures. In contrast, Schumacher and coworkers observed ATP-analogue binding. It is possible that the D309Q mutation stabilizes the complex or it may be that differences in crystallization conditions and in ATP-analogue concentration between our experiments and those described by Schumacher and coworkers are responsible for this discrepancy. The effect of the D309Q mutation should be easy to establish by obtaining the binding constants of native HipA–ATP and HipBA–ATP complexes and comparing these values with those published for the $HipA_{D309Q}$–ATP and $HipBA_{D309Q}$–ATP complexes (Schumacher *et al.*, 2009).

3.3. The tryptophan-binding pocket

During the model-building process, we noticed that both HipA monomer structures contain a pocket of structured but unassigned electron density surrounded by the side chains of Tyr37, Asn9, Arg39, Leu248, Leu250, Trp32 and Met8. We were able to fill this density with the three C-terminal residues of HipB: Leu84, Glu85 and Trp86 (Fig. 3). This arrangement of residues appears to be a little too perfect for a random peptide-binding site, especially taking into account the exquisite ion pairing between the C-terminal carboxyl of Trp86 and the guanidine of Arg39. The pocket maintains its shape in the previously published HipA structures even though there are no HipB residues modelled inside. Additional evidence comes from sequence alignment: conservation of sequence between HipB proteins from various species ends around residue 73, coincident with the end of the ordered polypeptide, but then unexpectedly picks up at the very C-terminus where a single tryptophan residue is perfectly conserved (Supplementary Fig. 1). At present, we can only guess at the significance of this pocket: it may be that it anchors the disordered portion of HipB to the surface of HipA, which in turn could lower the chances of proteolytic attack. Alternatively, the binding of Trp86 may modulate HipA activity (the ATP-binding site is ∼14 Å away). The significance of this pocket remains to be established experimentally by, for example, observing the effect of HipB C-terminal tryptophan mutations.

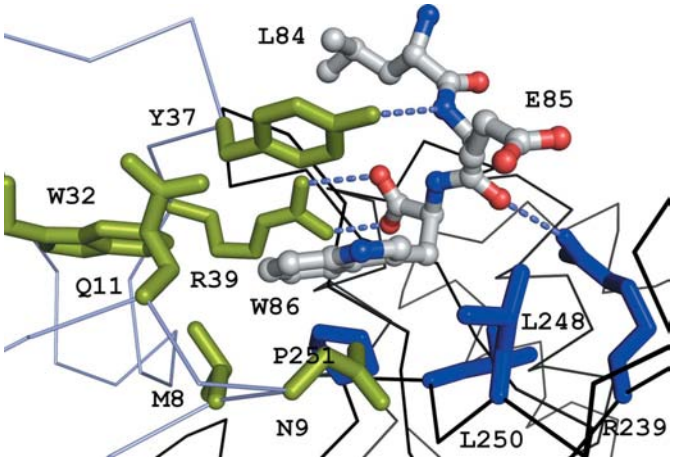

Figure 3
The tryptophan-binding pocket: the C-terminus of HipB is shown as a gray ball-and-stick model. HipA residues are colored blue (C-terminal domain) and green (N-terminal domain). Hydrogen bonds are represented by light blue dashed lines.

3.4. Proposed mechanism for HipA regulation

As mentioned above, the flexible region of HipA (residues 131–155) can adopt at least two distinct conformations. Unlike conventional kinase activation loops, this region contains a considerable stretch of structured polypeptide that constitutes part of the HipA core in either of the two observed conformations. We believe that its flexibility is biologically meaningful and that the two positions of the flexible region represent the two first steps in the HipA activation cycle. Our model of the activation process is built on the following data and assumptions: when the native HipBA complex is expressed the HipA protein is not phosphorylated and the complex is not toxic to the host cells. Therefore, we believe that the native HipBA complex contains a fully inactivated form of HipA. The conformation of the flexible region in this form of the protein agrees with the absence of Ser150 phosphorylation; it is impossible to imagine that the buried Ser150 would be accessible to either intermolecular or intramolecular phosphate transfer (Fig. 2). Furthermore, it is very unlikely that the 'off' conformation of the flexible region is possible with Ser150 in a phosphorylated state since the phosphate would experience severe steric clashes. The next step in the activation cascade may be illustrated by the conformation of the flexible region in HipA found in the mercury-derivatized complex (Fig. 2). In this form Ser150 is in close proximity to the γ-phosphate of ATP. Therefore, this 'activating' conformation resembles a transient state during which Ser150 undergoes phosphorylation. It is important to note that the exact conformation of the flexible region is probably not what is found in the mercury-derivatized HipBA complex since the latter does not contain bound ATP and therefore a portion of the flexible region invades the ATP-binding site. The Ala152 position can be adjusted so that Ser150 is still next to the ATP γ-phosphate, while steric clashes with the rest of the ATP molecule are removed. The final step in the activation cascade is the fully active HipA (with or without bound HipB) which has a third hitherto unobserved ('on') conformation of the flexible region. It is also possible that instead of a single conformation, the flexible region of the fully active HipA is disordered.

Since HipBA is not phosphorylated whereas HipA is fully phosphorylated when expressed in *E. coli* (MS data not shown), we think that HipB locks the flexible region of HipA in the 'off' conformation. It is not clear what the natural trigger for the activation process is: the mercury-induced change that we observed is probably a fortuitous artefact. If proteolysis of HipB has a trigger role (similar to other toxin–antitoxin pairs) then we agree with Schumacher and coworkers that it is very likely that the flexible C-terminal region of HipB is the site of the initial attack. There may even be a link between the tryptophan-binding pocket of HipA and the activation mechanism, assuming that the pocket has biological significance. It would be very interesting to mutate the C-terminal region of HipB and observe the effect of such a change on the activity and toxicity of HipA.

An alternative explanation of the peculiar behaviour of the flexible region may be proposed as follows: it may be that autophosphorylation of this element (after its primary cellular substrate has been mostly phosphorylated) results in the inactivation of the

enzyme, thus limiting the duration of HipA effects following its activation. This is an intriguing hypothesis which may explain how dormant cells ever emerge from their quiescent state without being subject to constant switch-off pressure by the activated HipA enzyme. We are grateful to the reviewers of this article for directing us towards this alternative hypothesis.

We would like to acknowledge Drs Richard Brennan and Maria Schumacher (University of Texas) for the helpful discussion. IV gratefully acknowledges the opportunity to pursue his summer internship with Pfizer Inc.

References

Abrahams, J. P. & Leslie, A. G. W. (1996). *Acta Cryst.* D**52**, 30–42.
Black, D. S., Irwin, B. & Moyed, H. S. (1994). *J. Bacteriol.* **176**, 4081–4091.
Black, D. S., Kelly, A. J., Mardis, M. J. & Moyed, H. S. (1991). *J. Bacteriol.* **173**, 5732–5739.
Brooun, A., Liu, S. & Lewis, K. (2000). *Antimicrob. Agents Chemother.* **44**, 640–646.
Davis, I. W., Leaver-Fay, A., Chen, V. B., Block, J. N., Kapral, G. J., Wang, X., Murray, L. W., Arendall, W. B. III, Snoeyink, J., Richardson, J. S. & Richardson, D. C. (2007). *Nucleic Acids Res.* **35**, W375–W383.
Emsley, P. & Cowtan, K. (2004). *Acta Cryst.* D**60**, 2126–2132.
Jayaraman, R. (2008). *J. Biosci.* **33**, 795–805.
Kussell, E., Kishony, R., Balaban, N. Q. & Leibler, S. (2005). *Genetics*, **169**, 1807–1814.
Lewis, K. (2008). *Curr. Top. Microbiol. Immunol.* **322**, 107–131.
Moyed, H. S. & Bertrand, K. P. (1983). *J. Bacteriol.* **155**, 768–775.
Moyed, H. S. & Broderick, S. H. (1986). *J. Bacteriol.* **166**, 399–403.
Murshudov, G. N., Vagin, A. A. & Dodson, E. J. (1997). *Acta Cryst.* D**53**, 240–255.
Otwinowski, Z. & Minor, W. (1997). *Methods Enzymol.* **276**, 307–326.
Perrakis, A., Morris, R. & Lamzin, V. S. (1999). *Nature Struct. Biol.* **6**, 458–463.
Schumacher, M. A., Piro, K. M., Xu, W., Hansen, S., Lewis, K. & Brennan, R. G. (2009). *Science*, **323**, 396–401.
Sheldrick, G. M. (2008). *Acta Cryst.* A**64**, 112–122.
Sun, P. D. & Radaev, S. (2002). *Acta Cryst.* D**58**, 1099–1103.
Sun, P. D., Radaev, S. & Kattah, M. (2002). *Acta Cryst.* D**58**, 1092–1098.
Terwilliger, T. (2004). *J. Synchrotron Rad.* **11**, 49–52.
Vaguine, A. A., Richelle, J. & Wodak, S. J. (1999). *Acta Cryst.* D**55**, 191–205.
Vonrhein, C., Blanc, E., Roversi, P. & Bricogne, G. (2007). *Methods Mol. Biol.* **364**, 215–230.